Journal of the Materials Science: Materials in Electronics, 2015, DOI 10.1007

Polarization switching at room temperature of undoped $BiFeO_3$ thin films crystallized at temperatures between $400 \leq T \leq 500$ºC

A. Perez-Rivero[1], M. Tomczyk[2], R .Jiménez[1], I. Bretos[1], J. Ricote[1], P.M. Vilarinho[2] and M.L. Calzada[1*]

[1]Instituto de Ciencia de Materiales de Madrid. Consejo Superior de Investigaciones Científicas, 28049 Madrid, Spain.

[2]Department of Ceramics and Glass Engineering, CICECO, University of Aveiro, 3810-93 Aveiro, Portugal.

*corresponding author: lcalzada@icmm.csic.es

Abstract. Pure $BiFeO_3$ perovskite thin films have been prepared on Pt-coated silicon substrates by chemical solution deposition at temperatures below 500ºC. Precursor solutions with and without Bi(III) excess have been used. Perovskite films without crystalline secondary phases, as detected by X-ray diffraction analysis, are obtained at the lowest temperature limit of 400ºC. However, the scanning electron micrographs of these films show surface microstructures formed by well defined grains surrounded by a fine grained phase, suggesting the appearance of a volume fraction of crystals in an early stage of crystallization. The films prepared with Bi(III) excess have better defined ferroelectric hysteresis loops than those without any excess, especially for the films annealed at 400ºC, which can be attributed to an improved connectivity of the ferroelectric phase. This together with the fact that leakage current densities in the films decrease with decreasing the processing temperature, make that the $BiFeO_3$ films prepared with Bi(III) excess and annealed at 400ºC and 450ºC can be poled at room temperature, obtaining an effective switching of the ferroelectric polarization with the electric field. Remanent polarization values of P_R~10 $\mu C/cm^2$ and P_R~60 $\mu C/cm^2$ with coercive fields of E_C~205 kV/cm and 235 kV/cm were obtained for the films prepared at 400ºC and 450ºC, respectively. The demonstration of the functionality at room temperature of these low temperature processed undoped $BiFeO_3$ thin films increases the interest in these materials for their integration in multiferroic devices.

Keywords: Bismuth ferrite; thin films; solution deposition; low temperature; ferroelectric, multiferroic.

1. Introduction

Bismuth ferrite ($BiFeO_3$) is a room temperature multiferroic material that exhibits ferroelectric and ferromagnetic ordering at room temperature in a single perovskite (ABO_3) phase [1]. The coupling between these ferroic orders is of interest to produce additional and novel functionalities with applications in devices (e.g., spintronics, electrically switchable magnets or magnetoelectric non volatile memories). However, the spontaneous polarization, P_S, values usually measured in bismuth ferrite materials are significantly smaller than the spontaneous polarization ~~those~~ expected for a ferroelectric with such a high Curie temperature, T_C (T_C~830 ºC, P_S up to 100 μC/cm^2). This is because of the high leakage current densities and dielectric losses of the material produced by the difficulty to prepare pure $BiFeO_3$ perovskite materials [2]. The $BiFeO_3$ perovskite is a metastable phase between 447ºC and 767ºC with respect to the bismuth-rich ($Bi_{25}FeO_{39}$) and the iron-rich ($Bi_2Fe_4O_9$) phases, the stable compounds on each side of the $BiFeO_3$ in the phase diagram. Formation of defects associated to the two oxidation states of the iron (Fe^{2+} and Fe^{3+}) and to the volatility of bismuth (melting point of Bi_2O_3 = 817ºC) are easily produced during the processing of $BiFeO_3$ materials. Nowadays , key applications of multiferroic compounds are envisaged for the material in thin film form [3]. High quality epitaxial BFO thin films have been prepared at temperatures over 500ºC by physical methods, with ferroelectric polarization of ~ 60 μC cm [4]. But these thin film processing methods are of difficult application in large are and/or flexible electronics, in spite of the high ferroelectric response of the epitaxial $BiFeO_3$ thin films. Solution deposition methods are an optimal choice for integrating films in macro-electronics, because they require low investment costs and are industrial scalable. Thus, solution derived polycrystalline $BiFeO_3$ thin films with well-defined ferroelectric and ferromagnetic responses (even larger that those obtained in epitaxial thin films) have been prepared at temperatures over 500ºC, [5-9] which is the maximum temperature permitted in the Si-technology integration routines [10].

For multiferroic materials, the coexistence of ferromagnetism and ferroelectricity in a single phase well above room temperature is required, not only for improving the functionality of the device, but also to reduce its operation cost. Multiferroic ceramic materials have, in addition, important applications for using in harsh environments because of their high T_C and magnetic Neel temperature (T_N of 370ºC for $BiFeO_3$) that permit them to preserve their functionalities at high temperatures. But also these ceramics are insensitive to radiation and are chemically stable under moderate acidic/basic pH conditions. Recently, ferroelectric layered Aurivillius bismuth-based layered perovskites have also been reported as potential room temperature single phase multiferroics, where both ferroelectric and ferromagnetic properties come from the inclusion of substantial amounts of magnetic ions into the ferroelectric crystal structure [11]. However, since room temperature single phase multiferroic compounds are scarce, heterogeneous materials systems have been traditionally used, where an artificial coupling between the electric and magnetic order parameters is designed [12].

In this work, we show the solution preparation of single phase $BiFeO_3$ thin films at lower temperatures than commonly used. The films were deposited from solutions with or without Bi(III) excess and crystallized by rapid thermal annealed in air at temperatures below 500ºC. Under these processing conditions, the temperature limit of formation of the pure $BiFeO_3$ perovskite films was reduced to 400ºC. Structural and microstructural characteristics of the films are shown. The crystallization of the films at temperatures below 500ºC strongly reduces the leakage current contribution, allowing ferroelectric switching and poling at room temperature. Values of the spontaneous polarization of P_S of ~ 13 μC/cm^2 and remanent polarization of P_R ~ 10 μC/cm^2 are obtained in the $BiFeO_3$ thin films annealed at 400ºC, temperature compatible with some large area and plastic substrates.

2. Experimental Procedure

Precursor solutions of $BiFeO_3$ were prepared as reported elsewhere [9]. Two solutions were obtained, with and without a 5mol% of Bi(III) excess. These solutions were spin-coated at 3000 rpm for 45 s onto $Pt/TiO_2/SiO_2/(100)Si$ substrates. Wet layers were dried on a hot plate at 350ºC/60s. Rapid thermal treatments (RTP, JetStar 100T JIPELEC) in static air (1 bar), were carried out at temperatures of 400ºC samples (400_ stoichiometric and 400x with Bi(III) excess), 450ºC samples (450_ and 450x) and 500ºC samples (500_ and 500x), with a soaking time of 60 s and a heating rate of 30ºC/s. Deposition, drying and RTP treatment were repeated up to a maximum of 10 layers to fabricate crystalline films with a thickness of between 300 and 350 nm.

The crystalline phases developed in the films were studied by X-ray diffraction, using a Siemens D500 powder diffractometer with a Cu anode (λ= 1.5406 Å). Surface and cross-section images of the films were obtained by a field emission gun scanning electron microscope (FEG-SEM, Nova Nanosem 230 FEI Company equipment, Hillsboro, OR). Thicknesses of the films were calculated from the cross-section images.
A planar array of capacitors was fabricated by sputtering Pt / Au top electrodes on the film surfaces, with diameter sizes between 140 and 640μm. The variation of the charge current density with the electric field (J-E) loops was measured, with an in-house made system based on a virtual ground circuit [13]. In this system, sinusoidal voltage waves with a maximum of amplitude of 25 V and at a frequency of 1 kHz were applied to the capacitors using an E33220A function generator coupled to a Tabor 9100 wide band

voltage amplifier. The loops were traced by a Tektronix TDS520 oscilloscope. This equipment joined to a home built cryostat equipped with micro-manipulators allowed the thin films hysteresis loops measurements in the temperature range 100-400K. Capacitance, finite resistance effects and non-linear leakage current densities are the origin of the non-switching contributions to these curves. These contributions were calculated and subtracted from the experimental J-E curves by a simulation model that uses a fitting algorithm based on an implemented hyperbolic tangent function for the simulation of the ferroelectric switching [14, 15]. The current response of a parallel (RC) circuit is also included to take into account the linear capacitance and the linear conductivity of the Ferroelectric thin film. For the non-linear leakage currents, the models proposed by Juan and Rose [16, 17] were used. The non-linear current density J uses the following simple expression:

$$J \propto V^n/d^3 \quad (1)$$

where d is the thickness of the film and n can change between $2.0 \leq n \leq 3.5$-in the case of space charge conduction limited leakage, before entering in the degradation region [18]. For tracing a hysteresis loop, a voltage sweep is applied to the sample and so the voltage changes fast with time. Therefore and in order to implement the equation (1), that is a d.c. function, in the loops it is necessary to introduce a threshold voltage. Above this voltage, the non-linear leakage currents begin to contribute to the current response at the time scale in the loop. Below this threshold voltage, linear conductivity contributions are only considered. Taking into account these considerations, current density coming from non-linear leakage current (J_l) is as follows [19]:

$$J_l = B.(V(t) - V_0)^n \quad (2)$$

where B is a proportionality constant that keeps information about the type of leakage involved, V(t) is the variation of the applied voltage with time, V_0 is the threshold voltage and n is an exponent with values between 2 and 3. In the proposed model, a simple approximation is made, fixing the value of the exponent n in all the voltage range used for tracing the loop. This is just a necessary simplification because the exponent can change with the applied voltage [18]. Here, a fixed exponent of n = 2.3 has been chosen, obtaining a good agreement for all the films. After the compensation of the loops by the fitting the leakage contributions for each sample can be extracted [19]. Polarization versus electric field loops (P-E ferroelectric hysteresis loops) were obtained by integration of the experimental J-E curves, whereas the integration of the calculated J-E curves without the non-switched contributions results in the compensated P-E ferroelectric hysteresis loops. Remanent and spontaneous polarization values (P_R and P_S), and coercive fields (E_C) were obtained from the loops for each of the films.

3. Results

3.1. Structure and microstructure

The effect of the annealing temperature on the crystallization in air of $BiFeO_3$ thin films prepared from precursor solutions with and without Bi(III) excess is shown in the X-ray diffraction patterns of Figures 1 and 2. In both cases, crystalline perovskite phase is not observed in the patterns of the films treated at 350ºC. However, the crystalline perovskite phase is detected in the 400ºC, 450ºC and 500ºC. Other reflections associated to secondary crystalline phases are only observed in the patterns of the films treated at 500ºC, for both films with and without Bi(III) excess. A small and broad peak at 2θ~28.2º is recorded (Figures 1a and 2a). This may be due to a nanocrystalline phase with composition close to $Bi_{25}FeO_{39}$ (JCPDS 46-0416 file), which is usually stabilized during processing at temperatures below 447ºC.[2] Therefore, it should be also present in the films prepared at lower temperatures, but probably not diffracting under X-rays due to its low crystallinity. Reflections of the $BiFeO_3$ perovskite are indexed in the patterns of Figures 1 and 2 to a rhombohedral (R3c) crystal structure (JCPDS-ICDD 86-1518 file). The 202 and 024 $BiFeO_3$ perovskite peaks appear overlapped to the 111 and 200 peaks of the Pt-bottom electrode (JCPDS-ICDD 4-802 file), respectively. Therefore, a detailed study of the patterns of Figures 1 and 2 was only carried out in the 2θ intervals of 21.0°-24.0° and 28.0°-34.0°, where the 012 and 104/110 reflections of the perovskite are recorded, respectively. The results obtained are summarized in the tables inserted in Figures 1 and 2. From them, an improvement in the crystallinity of the films can be hypothesized from the decrease of the broadening of the perovskite peaks and the splitting of the 104/110 reflections produced with the increase of the annealing temperature and the Bi(III) excess. It has to be noted, that these reflections appear in all of the films at slightly higher 2θ values than those of the JCPDS-ICDD 86-1518 pattern tabulated for the $BiFeO_3$ rhombohedral perovskite. This indicates smaller cell parameters of the $BiFeO_3$ perovskite film than the expected ones. This cell strain can result from the stresses induced by the substrate in the film during the deposition and crystallization processes [20]. The deviations are, in general, smaller as the annealing temperature increases and in the films prepared with Bi(III) excess that could be associated, not only to the stresses but also to a lower content of defects in the perovskite cell [2].

Figures 3 and 4 show the plan-view and cross-section FEG-SEM images of the $BiFeO_3$ thin films processed at temperatures between 400ºC and 500ºC, and without and with Bi(III) excess, respectively. The average thickness of the films is, for all of them, between 320 and 350 nm, not observing noticeable dissimilarities in the cross-section microstructure images. However, appreciable differences in microstructure are observed in the film surfaces. At the lowest annealing temperature, 400ºC, the film 400_ shows areas morphologically differentiated; zones with well defined grains surrounded by a fine grained phase (Figure 3). The former should correspond to the crystalline phase responsible of the perovskite reflections detected in the XRD pattern of Figure 1, whereas the latter should be an amorphous or nano - crystalline secondary phase with small contribution to the x-ray diagrams. As the annealing temperature increases, a large amount of grains seems to grow at the expense of the fine grained phase, leading to a final film microstructure at 500ºC with grains of a surface average size of ~195 nm. This grain growth results in an improvement of the crystallinity of the films, which is associated with the decrease of the full width at half maximum (FWHM) of the perovskite peaks as commented before, Figure 1. The films with Bi(III) excess follow a similar evolution of the surface microstructure with the annealing temperature (Figure 2 and 4). But, that processed at 400ºC, 400x, seems to be one step forward in comparison with the film without Bi(III) excess. They are formed by cluster of grains that convert into well defined grains with the increase of the annealing temperature. Thus at 500ºC, these films are formed by grains with an average size of ~135nm, slightly lower than those of the films with Bi(III) excess.

3.2. Electrical properties

3.2.1. J-E hysteresis loops

Due to the high leakage contributions in the $BiFeO_3$ thin films, ferroelectric characterization needs to be performed from low to room temperature in order to be able to switch the ferroelectric domains with large enough electric fields but without the occurrence of electrical breakdown. For all the samples, the temperature was lowered to 150K and then the amplitude of the sinusoidal electrical wave used for the measurements was increased slowly to prevent any irreversible conductivity degradation and to act as an electrical conditioning treatment. After observing switching in the loops, the temperature was increased in steps till 275 – 300 K, repeating the same measurement routine. Figures 5 shows the experimental J–E ferroelectric loops obtained for the films crystallized at different temperatures, prepared from solutions without and with Bi excess. Here, it is possible to observe the characteristic current maxima related to the switching of ferroelectric polarization for all the films.

The polarization of the films prepared with excess can only be switched at room temperature when crystallized at 400 and 450ºC (Figure 5 a, c). That prepared at 500ºC suffers dielectric breakdown during the switching loop measurement for temperatures higher than 225K, using the same maximum sinusoidal field (400 kV/cm), using the same maximum field a large enough electric field is applied, preventing the switching at room temperature (Figure 5 e). This occurs despite the well defined switching observed at 150-175K. Unlike them, none of the films prepared from solutions without excess polarization can be switched at room temperature. Actually, for the film prepared at 500ºC without excess polarization cannot be switched at temperatures larger than 200K; above these temperatures dielectric breakdown occurs (Figure 5 f). Moreover, a simple inspection of the ferroelectric switching current loops of Figure 5 indicates that on approaching room temperature, the contribution from non-linear leakage currents increases significantly in the films prepared with Bi excess (Figure 5 b, d, f), while they are not so important the rest of the films (Figure 5 a, c, e). Although dielectric breakdown is usually preceded by the appearance of non-linear currents, this is not the case for the $BiFeO_3$ prepared from solutions without any excess.

To extract more information from the loops of Figure 5, the fitting of the loops to the phenomenological model [14], as explained in the experimental section, has been performed. Figure 6 shows, as an example, the fitting of one of the previous J-E loops. In the plot, the experimental current density data (circles), the fitted current curve (thin line) and the calculated pure ferroelectric switching current curve (thick line) are shown. There is good agreement between the experimental data and the model used. The different parameters obtained from this fitting reveal relevant information about the electrical behavior of the films.

The spontaneous polarization values at increasing temperatures for all the films are presented in Figure 7a. The film prepared at 400ºC without any excess (400_) presents a spontaneous value of P_S = 5.3 μC/cm^2 at 150K, increasing to 11.2 μC/cm^2 at 200K, and slightly reducing the value at 250K to 11.0 μC/cm^2. When Bi excess is used in the precursor solution (400x), the behavior observed is similar but with a maximum value of P_S = 17.0 μC/cm^2 at 275K. At room temperature the value is 12.8 μC/cm^2. The evolutions with temperature of the coercive and bias voltages are also shown. The similar thickness of all films makes the comparison of the coercive and bias voltages of the films valid. The bias voltage values for the films crystallized at 400ºC mainly differs in its sign: -8 to -4V for the 400_ film and 4 to 2Vfor the 400x film. The coercive voltage and bias values are larger for the 400_ film. The results for the 450_ and 450x films (Figure 7a) indicate the same behavior of the spontaneous polarization that increases in both films with the temperature till maximum values, P_S = 43 μC/cm^2 at 225K and P_S = 71 μC/cm^2 at 250K for 450_ and 450x films, respectively. These values drop for higher temperatures: P_S = 40 μC/cm^2 at 250K and P_S = 62 μC cm^{-2} at 300K for 450_ and 450x films, respectively. The 450_ film presents larger coercive and bias voltage than the 450x film (Figure 7cFinally, the spontaneous polarization values of the 500_ and 500x films (Figure 7a) present a different behavior. The 500_ film shows an increase from P_S = 36 μC/cm^2 at 150K to 60 μC/cm^2 at 200K, while the 500x film shows a reduction from P_S = 80 μC/cm^2 at 150K to 69 μC/cm^2 at 225K. The coercive voltage is larger for the 500x film, with a small bias voltage (Figure 7d). The coercive voltage of the 500_ film increases with the temperature, while the bias voltage diminishes.

3.2.2 Leakage current curves

The leakage current curves are obtained from the fitting of the J-E hysteresis loops of Figure 5, and they are presented in Figure 8. They are not steady current curves, and thus, they cannot be compared directly with leakage currents, which are normally measured under D.C. conditions. Therefore, the discussion on the leakage behavior of the films will be only qualitative. The onset of non-linear leakage contributions in a short time interval (in this case, the corresponding to the loops frequency) must be attributed to the appearance of a degradation mechanisms. The value of the exponent n in equation (1) gives us information on the variations of the dependence of the current density and the applied voltage, which allows the identification, for example, of a transition region (characterized by a sharp current increase) which is attributed in the studies of steady state leakage current responses toa reversible breakdown of one of the Schottky barriers and the introduction of new charge transport mechanisms [21]. For higher voltages it has been determined that the current present a strong dependence on the applied voltage [21]. Besides, in order to ascertain any correlation between the film degradation and ferroelectric switching, the leakage curves are represented vs. the ratio between the voltage and the coercive voltage for each of them. It is known that the ferroelectric polarization has an important effect on the lowering of the Schottky barrier [22] The asymmetry produced in the applied voltages and the subsequent changes of the polarization states at the interfaces are taken into account by using for each branch (positive and negative) the value of the corresponding coercive field (Figure 8). Figure 8 a, c, and e correspond to the films prepared without any excess and b, d and e to those processed with Bi exces. In the following, for the leakage currents description, the positive voltage branches are used.

The leakage curves for the films 400_ and 400x are quite different. The observed response of the 400_ film is ohmic for all the voltages in the loop. This linear behavior as pointed out by Scott [23], can be related to the Simmons modified Schottky currents, which present a linear dependence with the field at the so-called low fields region of the I-V dependencies [21]. This model can also explain the observed differences in the leakage current behavior between the positive and negative voltage branches (see Figure 8). The current increases with the measuring temperature until dielectric breakdown for T > 250K. The opposite trend can be observed in the 400x films, which are subjected to a positive bias instead (Figure 7b). The behavior of the leakage with temperature indicates ohmic behavior is observed until 250K, temperature at which a change of the slope of the curve is observed for voltages in excess of the coercive voltage. At 275 and 300 K the response is non-linear with a n coefficient (equation 2) of 2.3. And no electrical breakdown is produced.

The leakage current behaviors of the films crystallized at 450ºC follow the same trends observed in the films crystallized at 400ºC. The 450_ film (Figure 8c) presents ohmic behavior without any evident change until 250K. However, a further temperature increase produces the electrical breakdown of the film when a large field is applied. The 450x film present ohmic behavior only till 225K (Figure 8d). At 250 K, a sharp slope change in the leakage curve for voltages 1.5 times the coercive voltage appears, and thus, for large voltages a non-linear behavior appears. This non-linearity dominates the leakage currents for larger temperatures until 300K, without reaching the electrical breakdown.

For the films crystallized at 500ºC, although similar behavior is observed, some differences are observed in the leakage current curves. In the 500_ film the ohmic behavior is observed till 175K, like for the rest of the films prepared from solution without any excess (Figure 8e). But at 200K the curve of this film shows a change in the slope at 1.5 times the coercive voltage, and for higher temperatures the dielectric breakdown is produced. The 500x film shows in the current curves this change of the slope even at 150K (Figure 8f) for voltages larger than two times the coercive voltage. In successive increases of the temperature, the voltage at which this change is observed decreases progressively: below two times V_C for 175 K, around V_C for 200K, and 0.7 times V_C for 250 K. For higher temperatures dielectric breakdown takes place.

4. Discussion

4.1 Ferroelectric switching behavior

The results show that the values of the polarization (P_S and P_R) are larger in the films prepared from solution with Bi excess, for the same crystallization temperature. When the structural characteristics and microstructures of films crystallized at the same temperature are compared, no significant changes can be observed that explain these differences. As the polarization values are related to the volume of ferroelectric phase that can be switched in the films, it must be assumed that the introduction of an excess of Bi in the precursor solution is increasing the volume fraction of defect-free, well-crystallized crystals. The volatility of Bi during processing may produce extensive defective regions, which do not segregate a measurable distinct phase, but they are most probably part of the grains, forming for example a core-shell structure. The decrease of the amount of these regions by the addition of Bi excess in the precursor solutions has also effects on the conduction mechanisms developed in the film, as it will be discussed later.

The process of increasing gradually the temperature while applying electric fields above the coercive value has a conditioning effect on the polarization of these films. $BiFeO_3$ has been reported to be dominated by the pinning of their ferroelectric domains [24]. The polarization switching contributes to the reorganization of point defects at a given temperature as a part of the conditioning effect. On increasing the temperature, the defect mobility increases, and thus, more domains can be switched for the same external field [25].

However, as soon as the non-linear contributions to the conduction appear, the polarization starts decreasing with the measuring temperature. This effect can be easily observed comparing the 400_ film that does not show any current non-linearity and its polarization increases with the measuring temperature, and 500x that shows non-linear contributions to the conductivity at all the temperatures and its polarization values only go down as measuring temperature increases. The large increase of the conductivity at large electric fields makes the application of an electric field on the film less effective, causing a subsequent decrease of the polarization values. This behavior cannot be attributed to the fact that the material is closer to the ferroelectric-to-paraelectric phase transition, which will cause polarization to be lower. For $BiFeO_3$ this takes place at quite high temperature (1170K) and it should produce only slight changes in the ferroelectric properties in the temperature interval used in the measurements.

In order to make a more specific comparison of the ferroelectric response of the films we have collected in Table I the results obtained from the hysteresis loops measured at 200K. At this temperature all the measured capacitors have been subjected to the same electrical conditioning and, thus, the electrical situation of all films is more comparable. Apart from the differences of the polarization values of the films prepared from solutions with and without Bi excess, already discussed, it is clear that the increase of the crystallization temperature, which in both cases produces films with larger and better crystallized grains according to the structural and microstructural results, leads to an increase of the polarization values and of the remanence of the films with an increase of the P_r/P_s ratio, accompanied by a strong decrease of the coercive fields. The size of the grains and the probable columnar growth in the films crystallized at 500ºC seems to hinder the formation of the interface phenomena that causes the appearance of internal bias in the films, which is maximum for the films with a fine grained phase crystallized at 400ºC. The nature of these interfaces seems rather inhomogeneous and the electric bias created can be of a variable sign in these films, as it can be seen in Table I. The influence of this differentiated microstructure of the films crystallized at 400ºC is also clear on the permittivity values, which are much smaller than for the films crystallized at larger temperatures and with a more homogeneous grain size distribution. However, this is not correlated to the conductivity values obtained, as these are related to the various conduction mechanisms found and that will be discussed in the following section.

4.2 Leakage currents.

The appearance of non-linear currents, reported for $BiFeO_3$ films [26-28], occurs at different temperatures for each of them. The activation of these new, non-linear charge transport mechanisms when the electric field increases, in the so called transition region [21], is accompanied by the breakdown of one of the Schottky barriers. It must be taken into account that the height of this barrier decreases with the polarization of the film. Therefore, the discussed increase of the polarization values with the temperature, together with the reorganization of the defects and their higher mobility, favors the appearance reduction of the barrier as we increase the measuring temperature. The evolution of the leakage currents with the temperature can be related to a Simmons modified Schottky mechanism. Then on increasing temperature there is an increase in the switched ferroelectric polarization and a reorganization of the point defects due to depinning of domains [28]. Therefore, we observe that the electric field at which the non-linear currents appear decreases as the measuring temperature increases.

The films crystallized at 400ºC and 450ºC have lower polarizations and, therefore, the barrier is not broken easily, and the non-linear currents only appear for the highest temperatures (above 250K). Unlike them, the films crystallized at 500ºC, with large grains and large polarizations, show non-linear conductivity behavior at temperatures as low as 150K. Similarly, we discuss the films prepared from solutions without Bi excess, which present lower values of the polarization and, in principle, more defects, as discussed before. This situation does not favor the easy breakdown of the Schottky barrier, and therefore, the appearance of non-linear currents is very limited and only significant for the highest temperature of the film crystallized at 500ºC.

The temperatures, at which the dielectric breakdown takes place, follow a similar trend to the appearance of non-linear currents. In principle, both phenomena must be related. It is observed that the dielectric breakdown occurs at lower temperatures as the crystallization temperature increases and for more defective films, prepared from precursor solutions without excess. In this case, the current is not limited by the bulk of the films, which may form current paths along less crystallized regions, and dielectric breakdown occurs without the previous development of extensive non-linear currents.

The hysteresis current loops of the film crystallized at 400ºC from a solution without any excess show less defined switching maxima than the same film from a solution with Bi excess (Figures 5 a, b). The shape of these maxima, together with the high coercive fields, indicates a worse connectivity of the ferroelectric phase for the films prepared without Bi excess [29]. As the thickness of all films is quite similar, the connectivity of the ferroelectric phase is related to the relative quantity of less crystalline phase in the films [29]. Connectivity is also related to the crystallization temperature, and while for the films crystallized and 400ºC large grains are surrounded by a fine grained phase (connectivity 0–3), this evolves to an increased crystallinity and a connectivity 1-3 in the films crystallized at 450ºC. This heterogeneous phase distribution supports the idea of the development of current channels, leading to a premature breakdown in these films. The improvement of the crystallinity in the films prepared with Bi excess, limits the effects of this connectivity. The addition of a volatile element for the preparation of ferroelectric thin films like $PbTiO_3$, also results in the improvement of their properties when crystallized at low temperatures [30]. It is assumed that the crystals formed have a core–shell structure with a less crystalline/ amorphous phase in the shell, which will be thicker if the disappearance of the volatile element (Bi of Pb) is not compensated by the addition of an excess in the precursor solution.

The control of the degradation mechanism in $BiFeO_3$ films finally allows that the films crystallized at 400 and 450ºC from solutions with Bi excess can be poled at room temperature with P_R values of 13 and 62 μC/cm^2, respectively. These films present the optimal connectivity of the ferroelectric phase that warrants functional properties as piezoelectricity [29]. These P_R values are of the same order as those obtained for traditional lead zirconate titanate ($Pb(Zr_{1-x}Ti_x)O_3$, PZT) [31-35] or doped $BiFeO_3$ thin films [36-40].

5. Conclusions

$BiFeO_3$ thin films with high values of remanent polarization at room temperature have been obtained at low crystallization temperatures: 62 and 13 μC/cm^2 for films prepared at 450ºC and 400ºC, respectively. To achieve it, precursor solutions using Bi excess have been used, which provide the films with the electric properties that make them potentially operative in microelectronic devices.

The preparation of these films at low temperatures produces microstructure with inhomogeneous grain size, and the coexistence of amorphous or less crystalline phases with full crystalline grains. It is shown that the addition of Bi excess increases the volume of crystalline ferroelectric phase in the film, and enhances the connectivity of the ferroelectric grains, which has a large impact on the ferroelectric behavior of the films.

The conductivity problems of $BiFeO_3$ films that usually lead to the dielectric breakdown when a large electric field is applied seems not necessarily related to the occurrence of large non-linear leakage currents. The conduction mechanisms found for thin films with more defects and lower polarization (prepared from solution without Bi excess) produce a dielectric breakdown at lower temperatures than thin films with a large volume fraction of full crystallized phase, but without the appearance of significant non-linearities in the current.

The successful low temperature processing of these lead-free, multiferroic films with accessible properties at room temperature is an important step further in the use of these materials in microelectronics applications, where an adequate functionality must be combined with the use of non-contaminant elements and processing protocols compatible with all the elements of the device.

Acknowledgements. This work has been funded by the COST-Action IC1208 and the Spanish Projects MAT2010-15365 and MAT2013-40489-P. A. Perez-Rivero acknowledges the support of the FPI Spanish program and I. Bretos of “Juan de la Cierva” Spanish program.

Table I. Results derived from the density current hysteresis loops measured at 200 K and 1 kHz.

Precursor solution	Crystallization temperature	P_R ($\mu C/cm^2$)	P_S ($\mu C/cm^2$)	P_R/P_S	E_C (kV/cm)	E_{bias} (kV/cm)	ε´	ρ (Ω×cm)
No excess	400°C	7.39	11.20	0.66	401	-333	330	0.5×10^7
	450°C	28.77	36.43	0.79	370	213	669	0.8×10^7
	500°C	57.10	63.60	0.90	180	53	783	0.2×10^7
Bi(III) excess	400°C	7.79	11.20	0.69	282	214	302	3.0×10^7
	450°C	52.50	65.60	0.80	270	181	789	0.6×10^7
	500°C	66.00	70.20	0.94	192	28	790	0.2×10^7

Figure captions:

Figure 1: X-ray diffraction results for BFO thin films without Bi excess. A) diffraction diagrams as a function of the annealing temperature. B) Zoom in the θ - 2θ region $21 \leq \theta \leq 24$ at temperatures where the phase appears. The inset is the diffraction peak position and width, and the expected position from the corresponding powder diffraction card. C) Zoom in the θ - 2θ region $28 \leq \theta \leq 33$ at temperatures where the phase appears. The inset is the diffraction peak position and width, and the expected position from the corresponding powder diffraction card.

Figure 2: X-ray diffraction results for BFO thin films with Bi excess. A) diffraction diagrams as a function of the annealing temperature. B) Zoom in the θ - 2θ region $21 \leq \theta \leq 24$ at temperatures where the phase appears. The inset is the diffraction peak position and width, and the expected position from the corresponding powder diffraction card. C) Zoom in the θ - 2θ region $28 \leq \theta \leq 33$ at temperatures where the phase appears. The inset is the diffraction peak position and width, and the expected position from the corresponding powder diffraction card.

Figure 3: Surface (left) and thickness (right) SEM micrographs of BFO films prepared at different annealing temperatures without Bi excess. A) annealing at 400ºC, B) annealing at 450ºC. C) annealing at 500ºC.

Figure 4: Surface (left) and thickness (right) SEM micrographs of BFO films prepared at different annealing temperatures witht Bi excess. A) annealing at 400ºC, B) anealing at 450ºC. C) annealing at 500ºC.

Figure 5: Current density hysteresis loops, traced at 1 KHz measured at different temperatures. A) BFO film without Bi excess annealed at 400ºC (400_). B) BFO film with Bi excess annealed at 400ºC (400x). C) BFO film without Bi excess annealed at 450ºC (450_). D) BFO film with Bi excess annealed at 450ºC (450x). E) BFO film without Bi excess annealed at 500ºC (500_). F) BFO film without Bi excess annealed at 500ºC (500x).

Figure 6: Example of the current density hysteresis loop fitting. Sample BFO film with excess annealed at 500ºC. Hollow circle, experimental density current loop. Thin line calculated density current loop. Thick line ferroelectric switching current loop.

Figure 7: a) Change with the measuring temperature of the spontaneous polarization for all the samples. b) Variation with the measuring temperature of the loops coercive voltage and bias voltage. Samples annealed at 400ºC. c) Variation with the measuring temperature of the loops coercive voltage and bias voltage. Samples annealed at 450ºC. d) Variation with the measuring temperature of the loops coercive voltage and bias voltage. Samples annealed at 500ºC.

Figure 8: Leakage currents extracted from the density current hysteresis loop as a function of temperature for all the samples. A) BFO film without Bi excess annealed at 400ºC (400_). B) BFO film with Bi excess annealed at 400ºC (400x). C) BFO film without Bi excess annealed at 450ºC (450_). D) BFO film with Bi excess annealed at 450ºC (450x). E) BFO film without Bi excess annealed at 500ºC (500_). F) BFO film without Bi excess annealed at 500ºC (500x). Insets show the same plots but with a linear scale of the currents.

References

1. G. Catalan, J. F. Scott, Adv. Mater. **21**, 2463 (2009)

2. S.M. Selbach, M.A. Einarsrud, T. Grande, Chem. Mater. **21**, 169 (2009)

3. R. Ramesh, N.A. Spaldin, Nature Mater., **6**, 21 (2007)

4. B.C Jeon, D. Lee, M.H. Lee, S.M. Yang, S.C. Chae, T.K. Song, S.D. Bu, J.G. Yoon, T.W. Noh, Adv. Mater. **25**, 5643 (2013).

5. S. Iakoviev, C.H. Sofferbech, M. Kuhnke, M. Es-Souni, J. Appl. Phys. **97**, 094901 (2005)

6. A.Z. Simoes, C.S. Riccardi, M.L. Cos Santos, F. Gonzalez-Garcia, E. Longo, J.A. Varela, Mater. Res. Bull. **44**, 1747 (2009)

7. V. Fruth, M. Popa, J.M. Calderón-Moreno, E.M. Anghel, D. Berger, M. Gartner, M. Anastasescu, P. Osiceanu, M. Zaharescu, J. Eur. Ceram. Soc. **27**, 4417 (2007)

8. A. Hardy, S. Gielis, H. Van den Rul, J. D'Haen, M.K. Van Bael, J. Mullens, J. Eur. Ceram. Soc. **29**, 3007 (2009)

9. C. Gutiérrez-Lazaro, I. Bretos, R. Jiménez, J. Ricote, H. El Hosiny, D. Pérez-Mezcua, R.J. Jiménez-Rioboó, M. García-Hernandez, M.L. Calzada, J. Am. Ceram. Soc. **96**, 3061 (2013)

10. International Technologies Roadmap for Semiconductors (ITRS), 2013 Update, http://www.itrs.net/Links/2012ITRS/Home2013.htm

11. L. Keeney, T. Maity, M. Schmidt, A. Amann, N. Deepak, N. Petkov, S. Roy, M.E. Pemble, R.W. Whatmore, J. Am. Ceram. Soc. **96**, 2339 (2015)

12. C.A.F. Vaz, J. Hoffman, C.H. Ahn, R. Ramesh, Adv. Mater. **22**, 2900 (2010)

13. D. Rivero, L. Pardo, R. Jiménez, Revista Cubana de Física, **26**, 169 (2009)

14. R. Jiménez, C. Alemany, M.L. Calzada, A. González, J. Ricote, J.Mendiola, Appl. Phys. A: Mater. Sci. Process. **75**, 607 (2002)

15. S.L. Miller, R.D. Nasby, J.R. Schwank, M.S. Rodgers, P.V. Dresendorfer, J. Appl. Phys. **68**, 6463 (1990)

16. T.P. Juan, S., Chen, J. Y. Lee, J. Appl. Phys. **95**, 3120 (2004)

17. A. Rose, Phys. Rev. **97**, 1538 (1955)

18. H.Hu, S.B. Krupanidhi, J. Mater. Res. **9** 1484 (1994)

19. R. Jiménez, R. Fernández, J. Ricote, "Leakage current compensation of ferroelectric hysteresis loops in ultrathin capacitors". Piezo 2009, Electroceramics for End Users, Zakopane, Poland (2009)

20. J. Mendiola, M.L. Calzada, P. Ramos, M.J. Martin, F. Agullo-Rueda, Thin Solid Films **315,** 195 (1998)

21. A. Sigov, Y. Podgorny, V. Vorotilov, A. Vishnevskiy, Phase Trans. **86**, 1141 (2013)

22. I. Pintillie, I. Vrejoiu, D. Hesse, G. Le Rhun, M. Alexe, Phys. Rev. B **75** 104103 (2007)

23. J.F. Scott, J. Phys. Condens. Matter **26** 142202 (2014)

24. T. Rojac, M. Kosec, B. Burdic, N. Setter, D. Damjanovic, J. Appl. Phys. **108**, 074107 (2010)

25. Y. Gao, K. Uchino, D. Viehland, J. Appl. Phys. **101,** 054109 (2007)

26. M. Alexe, C. Harnagea, D. Hesse, U. Gossele, Appl. Phys. Lett. **75**, 1793 (1999)

27. G.W. Pabst, L.W. Martin, Y.H. Chu, R. Ramesh, Appl. Phys. Lett. **90**, 072902 (2007)

28 I. Bretos, R. Jiménez, C. Gutiérrez-Lazaro, I. Montero, M.L. Calzada, Appl. Phys. Lett. **104**, 092905 (2014)

29. L. Pardo, J. Mendiola, C. Alemany, J. Appl. Phys. **84**, 5082 (1988)

30. C. de Dobbelaere, M.L. Calzada, R. Jiménez, J. Ricote, I. Bretos, J. Mullens, A. Hardy, M. van Bael, J. Am. Chem. Soc. **133**, 12922 (2011)

31. H.M. Alshareef, A.I. Kingon, X. Chen, X.R. Bellur, O. Auciello, J. Mater. Res. **9**, 2968 (1994)

32. W. Gong, J.F. Li, X. Chu, Z. Gui, L. Li., Acta Mater. **52**, 2787 (2004)

33. M. Mandeljc, B. Malic, M. Kosec, Integrated Ferroelectrics **52**, 205 (2003)

34. A. Wu, P.M. Vilarinho, I. Reaney, M. Miranda-Salvado, Chem. Mater. **15**, 1147 (2003)

35. I. Bretos, R. Jiménez, A. Wu, A.I. Kingon, P.M. Vilarinho, M.L. Calzada, Adv. Mater. **26**, 1405 (2014)

36. V.R. Singh, A. Garg, D.C. Agrawal, Appl.Phys.Lett. **92**, 152905 (2008)

37. H.Uchida, R.Ueno, H.Funakubo, S.Koda, J. Appl. Phys. **100**, 014106 (2006)

38. S.R. Das, P. Bhattacharya, R.N.P. Choudhary, R.S. Katiyar, J. Appl. Phys. **99**, 066107 (2006)

39. S.K.Singh, Thin Solid Films **527**, 126 (2013)

40. J.K. Kim, S.S. Kim, W.J. Kim, A.S. Bhalla, R. Guo, Appl.Phys.Lett. **88**, 132901 (2006)

Figure

Click here to download Figure: Figures_paper BFO films_16March2015.pptx

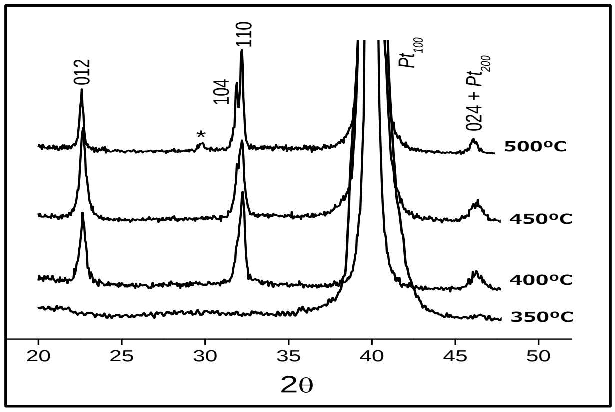

a)

Annealing temperature	$BiFeO_3$ film without Bi(III) excess [h k l]		JCPDS-ICDD 86-0416 $BiFeO_3$ (Rhombohedral R3c) [h k l]
	0 1 2		0 1 2
	2θ	FWHM	2θ
400 ˚C	22.670˚	0.422	22.417˚
450 ˚C	22.661˚	0.394	
500 ˚C	22.578˚	0.220	

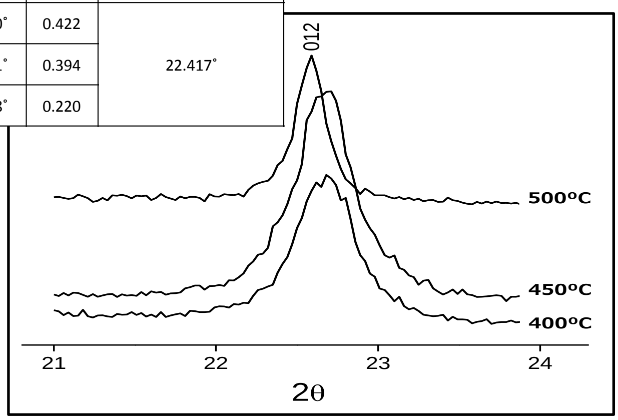

b)

Annealing temperature	$BiFeO_3$ film without Bi(III) excess [h k l]				JCPDS-ICDD 86-0416 $BiFeO_3$ (Rhombohedral R3c) [h k l]	
	1 0 4		1 1 0		1 0 4	1 1 0
	2θ	FWHM	2θ	FWHM	2θ	2θ
400 ˚C	31.912˚	0.386	32.233˚	0.304	31.754˚	32.069˚
450 ˚C	31.947˚	0.380	32.220˚	0.271		
500 ˚C	31.873˚	0.267	32.183˚	0.217		

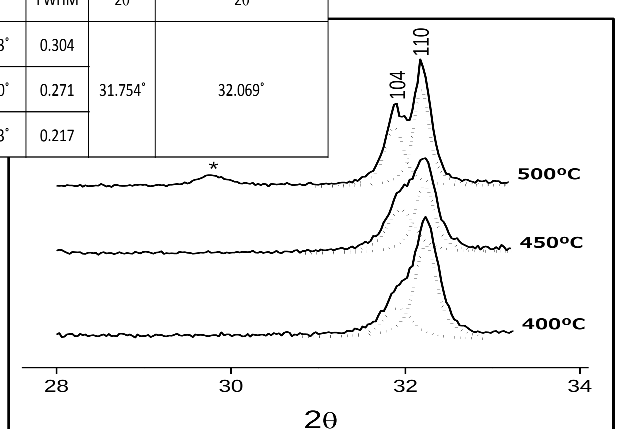

c)

Figure 1

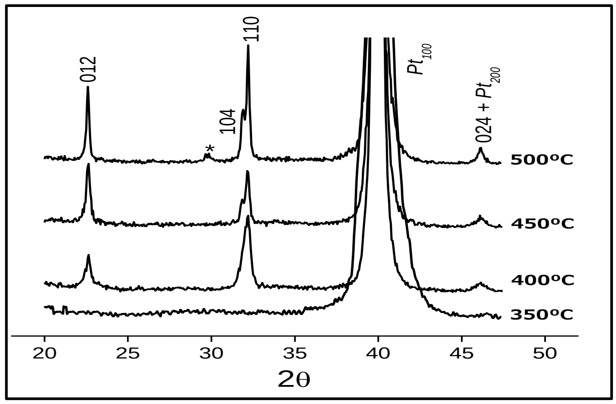

a)

Annealing temperature	$BiFeO_3$ film with Bi(III) excess [h k l]		JCPDS-ICDD 86-0416 $BiFeO_3$ (Rhombohedral R3c) [h k l]
	0 1 2		0 1 2
	2θ	FWHM	2θ
400 °C	22.583°	0.383	22.417°
450 °C	22.581°	0.284	
500 °C	22.609°	0.207	

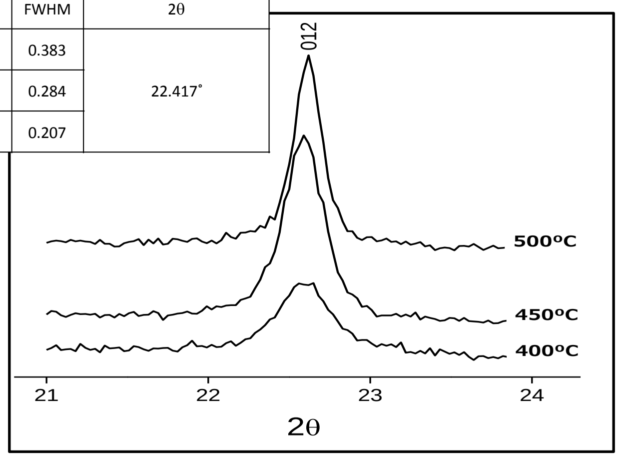

b)

Annealing temperature	$BiFeO_3$ film with Bi(III) excess [h k l]				JCPDS-ICDD 86-0416 $BiFeO_3$ (Rhombohedral R3c) [h k l]	
	1 0 4		1 1 0		1 0 4	1 1 0
	2θ	FWHM	2θ	FWHM	2θ	2θ
400 °C	31.877°	0.478	32.156°	0.394	31.754°	32.069°
450 °C	31.822°	0.255	32.131°	0.254		
500°C	31.909°	0.249	32.210°	0.195		

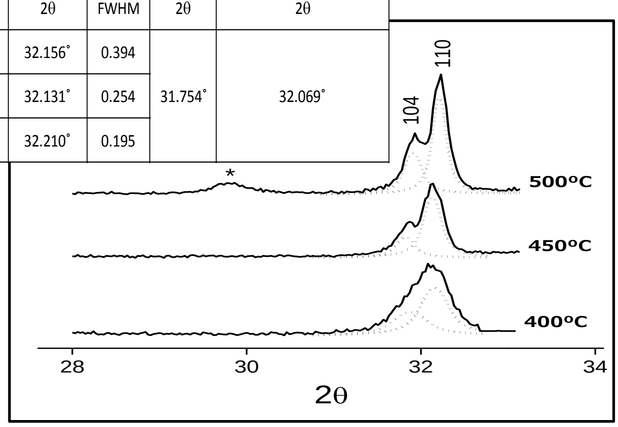

c)

Figure 2

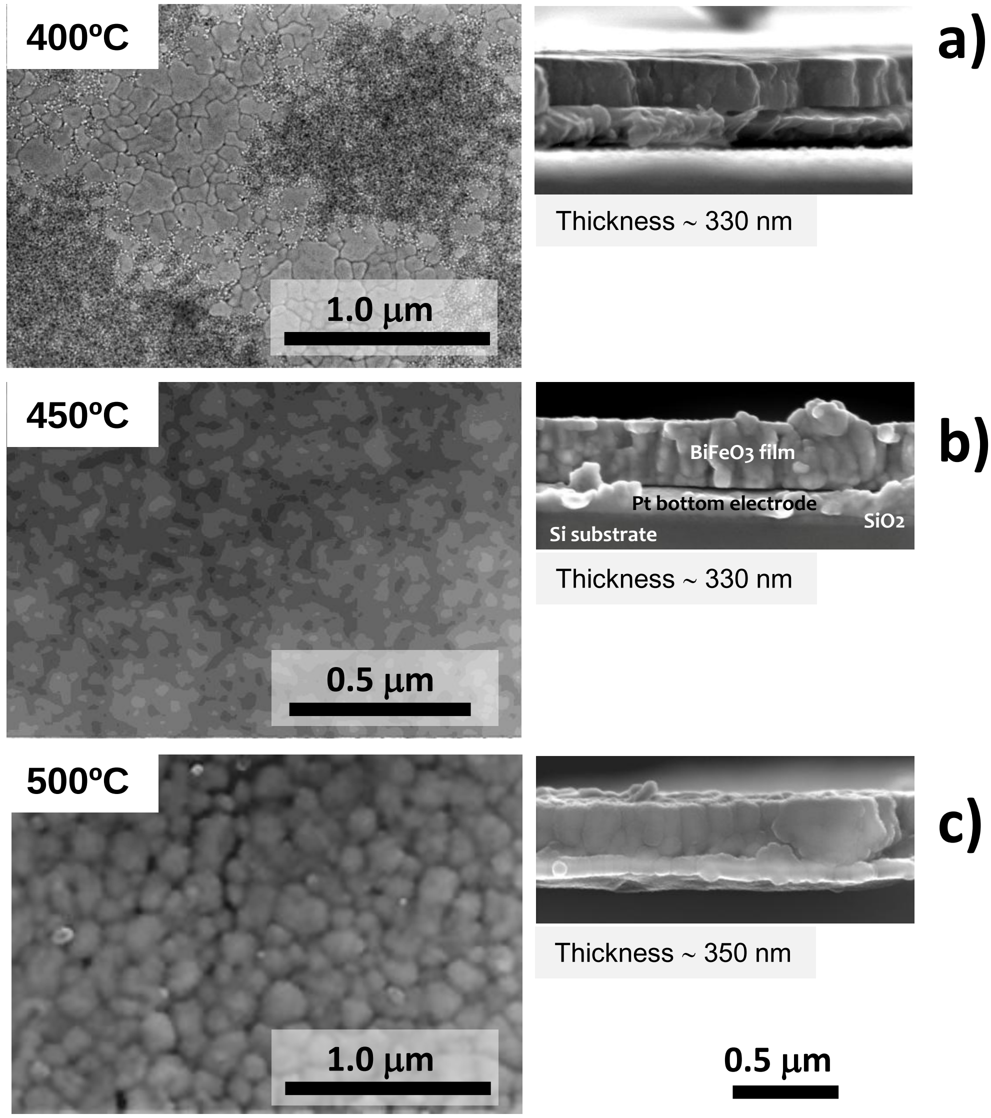
400ºC
1.0 µm
Thickness ~ 330 nm
a)
450ºC
0.5 µm
BiFeO3 film
Pt bottom electrode
Si substrate
SiO2
Thickness ~ 330 nm
b)
500ºC
1.0 µm
Thickness ~ 350 nm
c)
0.5 µm

Figure 3

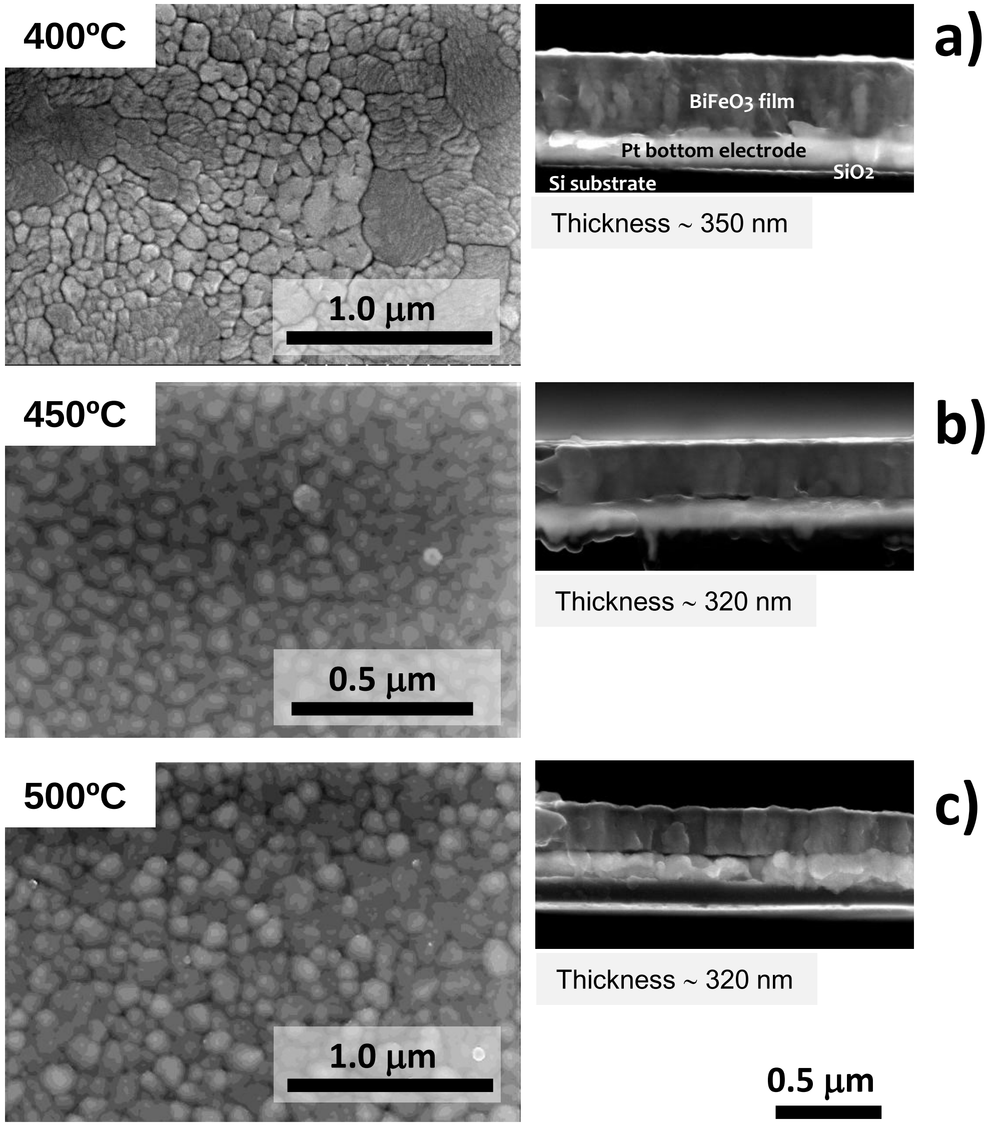
400ºC
1.0 µm
BiFeO3 film
Pt bottom electrode
Si substrate
SiO2
Thickness ~ 350 nm
a)
450ºC
0.5 µm
Thickness ~ 320 nm
b)
500ºC
1.0 µm
Thickness ~ 320 nm
c)
0.5 µm

Figure 4

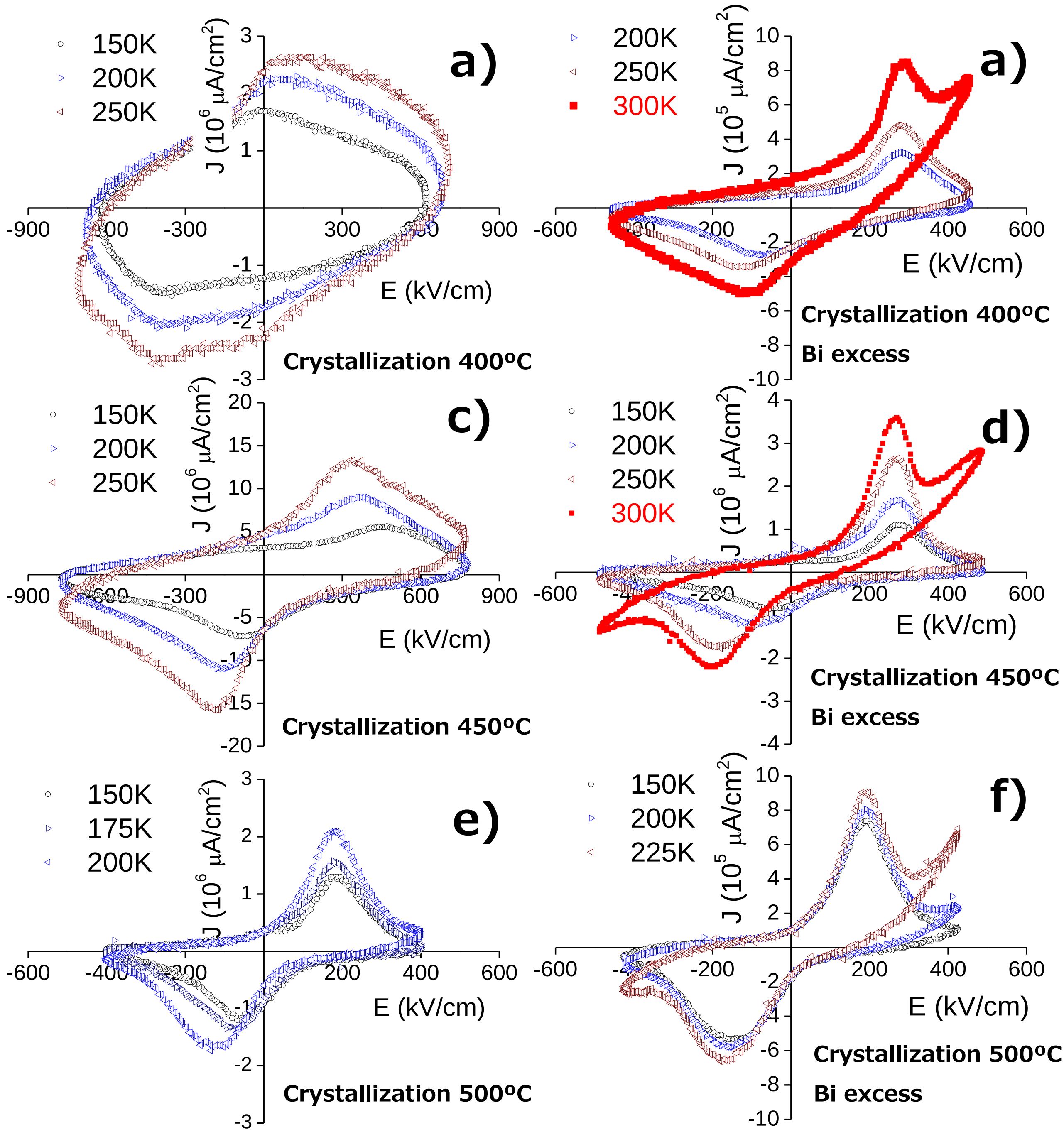
a)
150K
200K
250K
J (10^6 μA/cm^2)
E (kV/cm)
Crystallization 400ºC
a)
200K
250K
300K
J (10^5 μA/cm^2)
E (kV/cm)
Crystallization 400ºC
Bi excess
c)
150K
200K
250K
J (10^6 μA/cm^2)
E (kV/cm)
Crystallization 450ºC
d)
150K
200K
250K
300K
J (10^6 μA/cm^2)
E (kV/cm)
Crystallization 450ºC
Bi excess
e)
150K
175K
200K
J (10^6 μA/cm^2)
E (kV/cm)
Crystallization 500ºC
f)
150K
200K
225K
J (10^5 μA/cm^2)
E (kV/cm)
Crystallization 500ºC
Bi excess

Figure 5

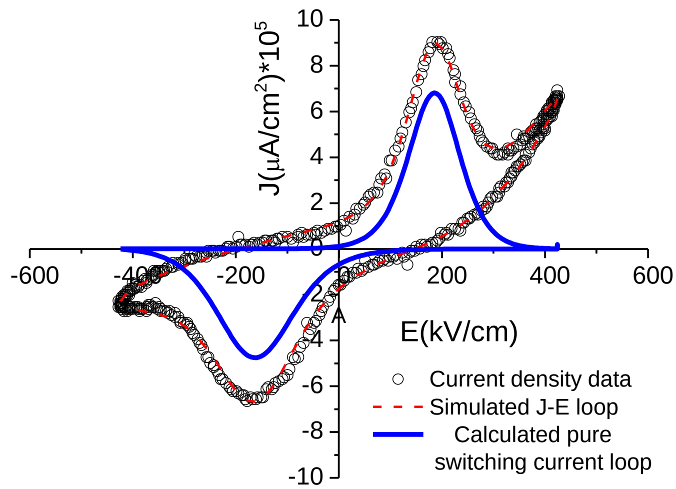

J(μA/cm2)*105
10
8
6
4
2
0
-2
-4
-6
-8
-10
-600
-400
-200
0
200
400
600
A
E(kV/cm)
Current density data
Simulated J-E loop
Calculated pure switching current loop

Figure 6

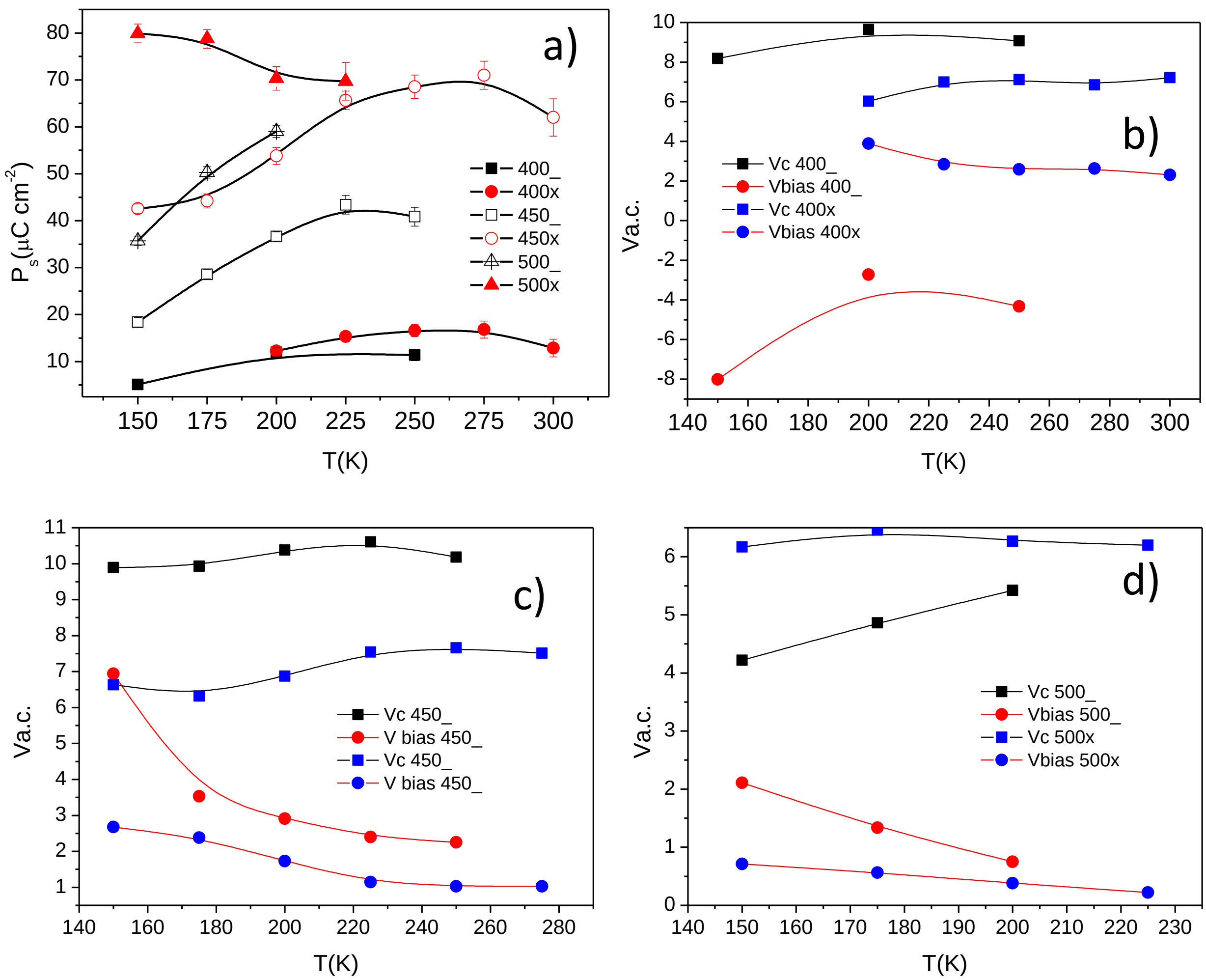
a)
80
70
60
50
40
30
20
10
P_s(μC cm^{-2})
150
175
200
225
250
275
300
T(K)
400_
400x
450_
450x
500_
500x
b)
10
8
6
4
2
0
-2
-4
-6
-8
Va.c.
140
160
180
200
220
240
260
280
300
T(K)
Vc 400_
Vbias 400_
Vc 400x
Vbias 400x
c)
11
10
9
8
7
6
5
4
3
2
1
Va.c.
140
160
180
200
220
240
260
280
T(K)
Vc 450_
V bias 450_
Vc 450_
V bias 450_
d)
6
5
4
3
2
1
0
Va.c.
140
150
160
170
180
190
200
210
220
230
T(K)
Vc 500_
Vbias 500_
Vc 500x
Vbias 500x

Figure 7

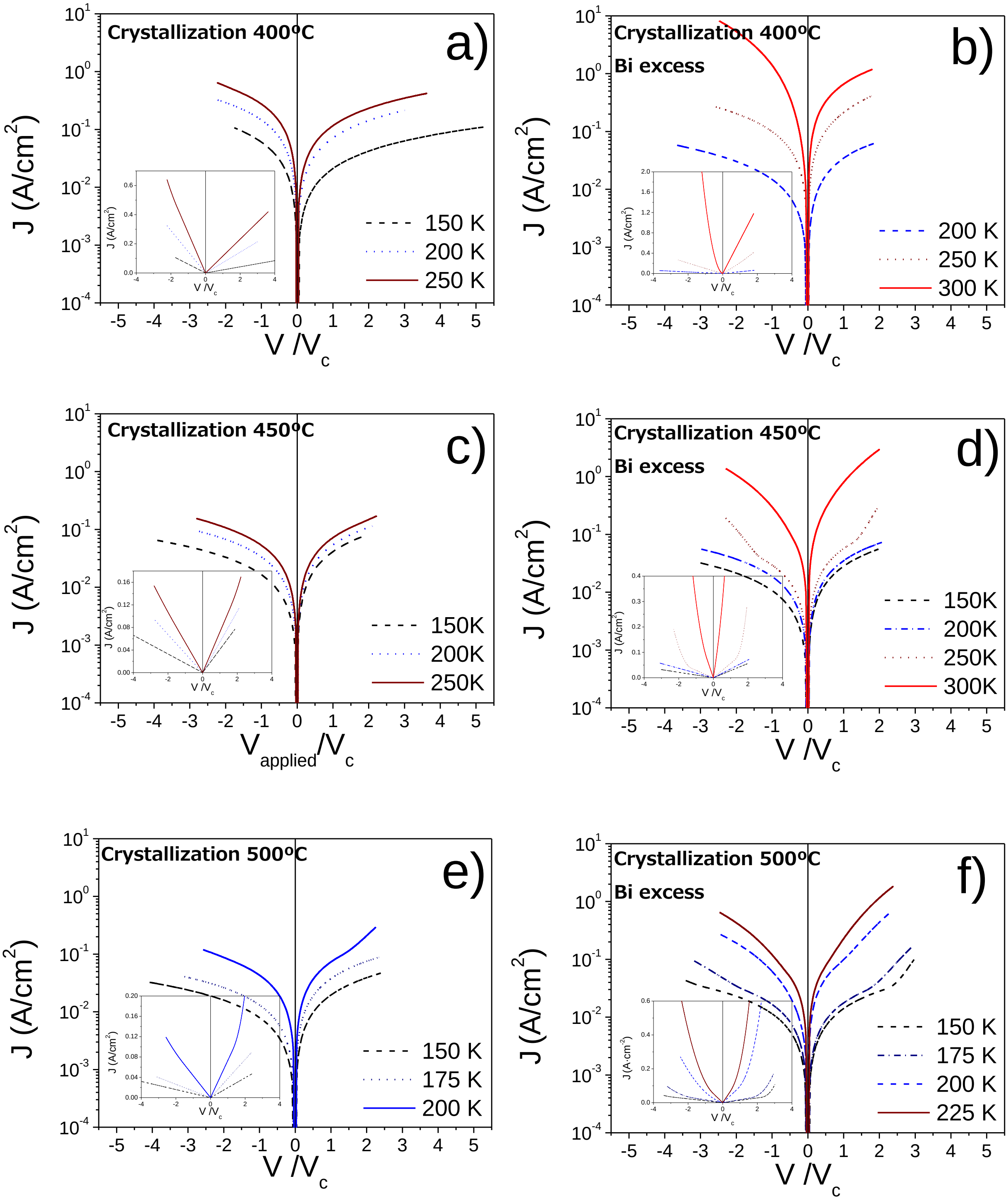

a)
Crystallization 400ºC
150 K
200 K
250 K
J (A/cm2)
V /Vc
b)
Crystallization 400ºC
Bi excess
200 K
250 K
300 K
J (A/cm2)
V /Vc
c)
Crystallization 450ºC
150K
200K
250K
J (A/cm2)
Vapplied/Vc
d)
Crystallization 450ºC
Bi excess
150K
200K
250K
300K
J (A/cm2)
V /Vc
e)
Crystallization 500ºC
150 K
175 K
200 K
J (A/cm2)
V /Vc
f)
Crystallization 500ºC
Bi excess
150 K
175 K
200 K
225 K
J (A/cm2)
V /Vc

Figure 8